Crosslinking by ZapD drives the assembly of short FtsZ filaments into toroidal structures in solution

Adrián Merino-Salomón[1], Jonathan Schneider[2], Leon Babl[1], Jan-Hagen Krohn[1,3], Marta Sobrinos-Sanguino[4], Tillman Schäfer[5], Juan R. Luque-Ortega[4], Carlos Alfonso[6], Mercedes Jiménez[6], Marion Jasnin[7]*, Petra Schwille[1]*, and Germán Rivas[6]*.

1- Department of Cellular and Molecular Biophysics, Max Planck Institute of Biochemistry, 82152 Martinsried, Germany.
2- Department of Molecular Structural Biology, Max Planck Institute of Biochemistry, 82152 Martinsried, Germany.
3- Exzellenzcluster ORIGINS, Boltzmannstr. 2, 85748 Garching, Germany.
4- Molecular Interactions Facility, Centro de Investigaciones Biológicas Margarita Salas, Consejo Superior de Investigaciones Científicas (CSIC), 28040 Madrid, Spain.
5- Cryo-EM facility, Max Planck Institute of Biochemistry, 82152 Martinsried, Germany.
6- Centro de Investigaciones Biológicas Margarita Salas, Consejo Superior de Investigaciones Científicas (CSIC), 28040 Madrid, Spain.
7- Helmholtz Pioneer Campus, Helmholtz Munich, 85764 Neuherberg, Germany; Department of Chemistry, Technical University of Munich, 85748 Garching, Germany.

*Corresponding authors

Correspondence: marion.jasnin@helmholtz-munich.de (M.S.); schwille@biochem.mpg.de (P.S.) ; rivas@cib.csic.es (G.R.)

Abstract

In most bacteria, division depends on a cytoskeletal structure, the Z ring, which serves as a scaffold for recruiting additional proteins, with which it forms the machinery responsible for division, the divisome. The detailed architecture of the ring, in particular the mechanisms of assembly, stabilization, and disassembly, are still largely unknown. Here, we highlight the role of FtsZ-associated proteins (Zaps) in stabilizing the Z ring by crosslinking the filaments. Among Zap proteins, ZapD binds the C-terminal domain of FtsZ, which serves as a hub for its regulation. We demonstrate that ZapD crosslinks FtsZ filaments in solution into toroidal structures formed by an arrangement of short, curved filaments. Using cryo-electron tomography combined with biochemical analysis, we reveal the three-dimensional organization of FtsZ within the toroids, shedding light on the crosslinking mechanism by ZapD. In spite of the compositional simplicity of our reconstituted system, the structural organization of the FtsZ polymers by ZapD appears to be compatible with the current model of the Z ring in the bacterial cell.

Introduction

Bacterial cell division is mediated by a multiprotein complex known as the divisome[1–3]. The components of the divisome interact reversibly to form a division ring that drives cytokinesis. The FtsZ protein, a structural homolog of eukaryotic tubulin with which it shares its GTPase and polymerization activities, is central to this process in most bacteria[4,5]. FtsZ is the main component of the Z ring, a structure formed at mid-cell during cell division, which provides a scaffold for recruiting other division proteins and is supposed to be essential for constricting the membrane[6–8]. Z ring formation requires FtsZ polymerization to form single-stranded filaments, which depends on the GTPase activity of FtsZ. GTP binding and hydrolysis induce

a conformational change in each monomer that modifies its binding potential, enabling them to follow a treadmilling behavior, similar to that of actin filaments.[9–13]. In response to environmental conditions, FtsZ filaments can further assemble into various structures such as bundles, sheets, toroids, or spirals[11,14–17].

The molecular components involved in cell division must be in the right place at the right time during the cell cycle. Several factors in this spatiotemporal regulation modulate FtsZ assembly. In *Escherichia coli*, FtsA and ZipA tether FtsZ to the membrane[18–20] and, together with a set of FtsZ-associated proteins (Zaps), stabilize the ring[21–25]. Conversely, negative modulators inhibit FtsZ assembly at other sites, namely Min proteins at the polar regions[26] and SlmA on the nucleoid[27]. Most of these modulators interact with FtsZ through its carboxy-terminal end, which acts as a central hub that modulates division assembly[28–30].

To date, a high-resolution structure of the Z ring is still missing. Most data support an arrangement of short FtsZ filaments distributed in patches along the equatorial circle, and held together by their lateral interactions and interactions with Zap proteins[2,7,31–33]. Cross-linking of filaments by Zaps is critical to maintain the juxtaposed organization of filaments into a ring structure, which may also be relevant to the functionality of the divisome and to the mechanism of force generation in cytokinesis[1,3,7,34–38].

Zap proteins have overlapping functions in stabilizing the Z ring within dividing cells. Individually, they are dispensable for division, though resulting in less compact Z rings in the absence of individual genes, while co-knock-out of two or more Zaps leads to cell elongation[21–23,39,40]. The different Zap proteins share no sequence homology, and their structure and mechanism of filament crosslinking differ[22,25,41,42]. Zap proteins may also participate in the active removal of FtsZ from the septum at the final stage of constriction[43,44] and in guiding the Z ring to the replication terminus region of the chromosome, through interaction with MatP to form the scaffolding anchor called Ter-linkage[45].

ZapD is the only Zap protein known to crosslink FtsZ by binding its C-terminal domain, suggesting a key stabilizing function of the Z ring structure[21,41,42,46–48] (Fig. 1a). ZapD is a symmetrical dimer consisting of an α-helical domain and a β-sheet domain containing a positively charged binding pocket required for crosslinking and bundling FtsZ filaments[42,48]. ZapD binds to the C-terminal region of FtsZ through electrostatic interactions[48]. ZapD crosslinks FtsZ filaments, promoting bundling and significantly reducing the GTPase activity of FtsZ[21]. The mechanism underlying the bundling of FtsZ filaments is still unknown, although a model of how ZapD crosslinks adjacent FtsZ filaments has been proposed based on the structural analysis of ZapD-FtsZ interactions[42]. In this model, the ZapD dimer connects two FtsZ filaments through the C-terminal domain, which could organize them in a parallel or antiparallel orientation due to the flexibility provided by the flexible linker (Fig. 1a). However, the experimental validation of this model is still missing. Characterizing how ZapD crosslinks FtsZ filaments can shed light on the molecular mechanism behind Z ring assembly.

Here, we used cryo-electron microscopy (cryo-EM) and cryo-electron tomography (cryo-ET) combined with biochemical and biophysical assays to study the structural organization of FtsZ polymers in the presence of ZapD. This integrated approach revealed that ZapD promotes the assembly of FtsZ filaments into toroidal polymers in solution, which is consistent with the low resolution structure of the Z ring visualized *in vivo*[7,49–51]. Our findings allowed us to propose a

molecular mechanism that leads to toroid formation, providing valuable information for understanding Z ring stabilization driven by crosslinking of division proteins.

Results

ZapD dimer interacts with FtsZ-GDP oligomers

Previous structural studies identified a direct interaction of ZapD through the C-terminal domain or central hub of FtsZ, finding charged residues involved in the interaction[46,48]. To independently confirm these results, we studied the interaction between FtsZ-GDP and ZapD by analytical ultracentrifugation (AUC) (Supplementary Fig. 1). First, we confirmed that ZapD forms stable dimers (Supplementary Fig. 1a (I) and b), in agreement with previous studies[21,46–48]. On the other hand, unpolymerized FtsZ-GDP self-assembled from monomers into dimers and other oligomeric species in small proportion, as expected[52] (Supplementary Fig. 1a (II)). When the two proteins were mixed, they formed hetero-complexes with a binding stoichiometry of 2 molecules of ZapD per FtsZ (Supplementary Fig. 1a (III-IV) consistent with the proposed interaction model[42]. In addition, we also confirmed the interaction of both proteins by fluorescence anisotropy and fluorescence correlation spectroscopy (FCS) (Supplementary Fig. 2a and b). In these experiments, an increase in fluorescence anisotropy or diffusion time, respectively, suggests the formation of larger particles as a result of protein-protein interactions.

ZapD binding promotes the bundling of FtsZ-GTP polymers

ZapD acts as a crosslinker of FtsZ filaments promoting bundling in solution[21], although the molecular mechanism of how ZapD crosslinks filaments remains elusive. To decipher the biochemical features underlying the bundling process, we analyzed the dependence of the formation of large FtsZ bundles or high-order FtsZ polymer structures on ZapD concentration using turbidity measurements at 350 nm. GTP-FtsZ (5 or 10 µM) filaments had negligible turbidity like ZapD alone (1 - 40 µM). However, upon the addition of ZapD, the turbidity of FtsZ polymers increased to reach a maximum signal at around 10 µM ZapD (ZapD-FtsZ molar ratio of around two), the level of which did not change significantly at higher ZapD concentrations assayed (40 - 80 µM, equivalent to a ZapD-FtsZ molar ratio from 8 to 16) (Fig. 1b and Supplementary Fig. 3).

Additionally, ZapD-driven FtsZ filament crosslinking resulted in a significant decrease in the GTPase activity of FtsZ, reaching 20% at equimolar or higher ZapD concentrations in the sample (Fig. 1c, Supplementary Fig. 4), in agreement with previous studies[21]. The formation of bundles at different buffer and protein conditions showed a dynamic behavior (Supplementary Fig. 3). These structures disassembled over time even before the exhaustion of GTP, which suggest a transient interaction with ZapD. However, recurrent replenishment of GTP allowed partial recovery of the turbidity signal, suggesting rapid reassembly of the FtsZ bundles (Supplementary Fig. 3e).

To determine the correspondence of the concentration dependence of the steady-state turbidity (linked to the formation of FtsZ bundles or high-order structures driven by ZapD; Fig 1b) to the amount of ZapD bound to the FtsZ binding sites, we employed the analytical centrifugation sedimentation velocity assays previously used to characterize the binding of

ZapD to GDP-FtsZ. This assay allowed us to separate ZapD-FtsZ bundles from ZapD free in solution and calculate the concentration of the unbound ZapD from the interference signal of the slowly sedimenting protein, which is behind the rapid sedimentation of the heavy ZapD-FtsZ complexes. Using this value of free ZapD and the known input concentrations of ZapD and FtsZ, we can compute the concentration of bound ZapD and the binding density of ZapD in the bundle (moles of ZapD dimer bound per mole of FtsZ monomer) at a given ZapD total concentration. We found that the bundles formed in the 5 - 10 µM ZapD region contained an estimated ZapD binding density of around 0.2 (one ZapD dimer for every four-six FtsZ monomers), while the ZapD density at the bundle in the 30 - 40 µM ZapD region was 0.5 (one ZapD dimer for every two FtsZ monomers). These results are consistent with parallel co-sedimentation assays and further analysis by SDS-PAGE showing enrichment of ZapD in the pellet containing the FtsZ bundles at high ZapD concentrations (Supplementary Fig. 5).

These findings show that the ZapD binding density in the polymers increases with ZapD concentration. We next carry out cryo-EM and ET studies to determine if this feature may impact the structural organization of the bundles formed.

ZapD facilitates the formation of FtsZ-GTP toroidal high-order structures.

Previous studies have visualized bundles with similar features by negative-stain transmission electron microscopy [21,42,48]. Here, cryo-EM enabled us to avoid any staining artifact or structure distortion due to adsorption or flattening upon drying of the grid[53], as well as to resolve single filaments. In the presence of GTP, FtsZ polymerized into thin filaments of variable length and curvature (Fig. 2a). Upon adding equimolar amounts of ZapD, corresponding to the subsaturating ZapD binding densities described in the previous section, FtsZ filaments assembled into bundles that predominantly form circular toroidal structures (Fig. 2b, c and Supplementary Fig. 6a), making them a compelling study target. A close-up view of the FtsZ toroid suggests a partially ordered arrangement of filaments in the toroidal structure (Fig. 2c).

Quantitative analysis of the toroidal structure showed a conserved organization, with an outer diameter on the order of the bacterial cell size (502 ± 55 nm) (Fig. 2d), a typical thickness of 127 ± 25 nm (Fig. 2e) and an average height of 93 ± 15 nm (Supplementary Fig. 6b). By measuring the shortest and longest axes, we determined that the circularity of the structure was 0.92 ± 0.1 and 0.85 ± 0.1 for the outer and inner diameters, respectively (Supplementary Fig. 6c). This conserved toroidal structure could derive from the intrinsic curvature of the FtsZ filaments[11,31,38] stabilized by ZapD binding.

Our data demonstrated that ZapD dimers crosslink adjacent FtsZ filaments into bundles and toroidal structures. These toroids are remarkably regular in size, and similar to the bacterial diameter[7,49,51,54]. This indicates that the inherent curvature of the FtsZ filaments is preserved across a range of ZapD bonds[38].

3D structure of ZapD-mediated FtsZ toroids revealed by cryo-ET

Visualization of toroidal FtsZ structures using cryo-EM suggested a regular arrangement of FtsZ filaments within the toroid (Fig. 2c). We then used cryo-ET to reveal their three-dimensional (3D) organization with greater precision. We first analyzed ZapD-mediated

toroidal FtsZ structures at equimolar concentrations in the sample (Fig. 3 and Supplementary Fig. 7a).

Cryo-ET revealed the dense packing of the toroidal structures, with numerous densities connecting the FtsZ filaments in all directions (Fig. 3a-c, Supplementary Figs. 7a and 8a). Zoomed-in views of the toroids in the XY plane showed that the toroid consists of rather short filament segments arranged almost parallel to each other (Fig. 3b and Supplementary Fig. 8a). However, cross-sectional views of the toroids revealed elongated structures rather than filament cross-sections along the Z-axis (Fig. 3c left, Supplementary Fig. 9a). We then extracted the toroid isosurface from the tomograms to precisely visualize its 3D structure (Fig. 3c right-e, Supplementary Fig. 8b-e and Supplementary video 1). The isosurface confirmed the presence of extended structures along Z, with much greater elongation than expected from the missing wedge effect on single FtsZ filaments (for comparison, see Supplementary Fig. 10). The vertically extended structures appeared to correspond to filaments connected or decorated by additional densities along the Z-axis (Supplementary Fig. 9b). These densities were only observed in the presence of ZapD (Supplementary Fig. 10b), suggesting that they are ZapD connections (Fig. 3e and supplementary Fig. 8e and 9b). Taken together, these results indicate that toroids are built and stabilized by ZapD-FtsZ interactions that can be established in all directions.

ZapD plasticity is essential for toroid shape and stabilization

Next, we manually labelled the connecting densities in the toroid isosurfaces to study their arrangement and connectivity with the FtsZ filaments (Fig. 4a; Supplementary Movie 2). We note that the high density of the toroids and the wide range of conformations of the densities in these structures prevented the use of subtomogram averaging to resolve their structure and spatial arrangement in the toroids. Most connections showed a characteristic bi-spherical shape between the filaments, reminiscent of ZapD dimers (Fig. 4 b-d). We found lateral linkages between two parallel FtsZ filaments at the same toroid height (Fig 4. b). FtsZ filaments at different heights can connect diagonally through ZapD proteins as bridging units, forming a complex 3D mesh (Fig. 4c, d and Supplementary Movie 2). We also identified the presence of putative ZapD proteins decorating a single FtsZ filament, which can be used to connect other nearby filaments (Fig. 4b). In addition, more than one crosslink between two filaments occurs, allowing stronger attachment between the filaments (Fig. 4d). Estimation of the precise number of ZapD molecules per FtsZ or the number of bonds per filament is difficult due to their intrinsic heterogeneous organization. However, we could observe a high number of connections stabilizing the toroidal structure, which correlates with the increase in ZapD binding density at higher ZapD concentrations, as discussed in the next section.

Visualization of the filament organization in 3D showed that the toroid is formed by an arrangement of short, highly crosslinked filaments, forming a dense 3D mesh (Fig. 4a and Supplementary Fig. 8e, 9b and 11). The short filament length, resulting in gaps between concomitant filaments, does not correlate with a higher number of ZapD connections (Supplementary Fig. 11), indicating that ZapD is able to crosslink filaments in all directions through transient interactions without causing filament breakage. This could play an important mechanistic role in the fuctionality of the FtsZ macrostructures.

Visualization of ZapD-mediated FtsZ toroidal structures by cryo-ET provided crucial information on the 3D organization, connectivity and length of filaments within the toroid. Our

data indicated that toroids consist of an arrangement of short FtsZ filaments connected by ZapD dimers in all directions, resulting in a conserved toroidal structure that is observed for the first time following the interaction between FtsZ and one of its natural partners *in vitro*.

High concentrations of ZapD promote the structural reorganization of FtsZ polymers into straight bundles

Once we characterized the FtsZ high-order structures promoted at lower ZapD binding densities, we addressed the impact of increasing the ZapD density on the structural organization of the ZapD-FtsZ polymers. At high concentrations of ZapD (typically 40 - 60 µM representing a molar ratio of one to six to FtsZ), we observed the formation of straight bundles with striated patterns between the FtsZ filaments (Supplementary Fig. 12), as well as the presence of some toroidal structures (Supplementary Figs. 6a). Here, the high concentration of ZapD molecules increased the number of links between filaments and ultimately promoted the formation of straight bundles, indicating that the assembly of FtsZ-ZapD structures is a reversible process that strongly depends on the amount of ZapD proteins crosslinking the filaments. Toroids and curved bundles always coexist, but the predominance shifts from toroids to straight bundles at high ZapD concentrations, which implies that the number of transient crosslinks between filaments modulates the features of the assembled high-order structures, resulting in the reorganization of the toroidal structures to form straight bundles upon saturation of ZapD (Supplementary Fig. 12). We then explored how higher densities of ZapD lead to the formation of straight bundles using cryo-ET.

Using the same approach to visualize the toroids, we collected tomograms of the straight bundles and extracted their isosurfaces (Fig. 5a, Supplementary Fig. 7b, and Supplementary Movie 3). The straight bundles are formed at high ZapD concentrations and consist of a highly organized stack of well-aligned FtsZ filaments (Fig. 5b). The connection of filaments by multiple putative ZapD proteins results in the straightening of the structure of the filaments[11,38] (Fig. 5c). Interestingly, ZapD seems to crosslink FtsZ filaments from the top or the bottom, rather than laterally, forming a row of ZapD proteins interacting with both filaments (Fig. 5d). Here too, structural analysis by subtomogram averaging was not possible due to the crowding, preferential orientation, and heterogeneity of the connections. The distance between ZapD proteins provided a mean value of 4.5 ± 0.5 nm (Supplementary Fig. 13a), consistent with the size of FtsZ proteins[13]. This observation suggests that most FtsZ proteins interact with the ZapD dimers that crosslink the filaments, in agreement with the ZapD enrichment in the bundles observed by sedimentation assays (Supplementary Fig. 5). On the other hand, we found that the presence of ZapD increased the distance between two FtsZ filaments connected by ZapD proteins compared with the spacing in the absence of ZapD, regardless of the amount of ZapD connections (from 5.9 ± 0.8 nm to 7.88 ± 2 nm in toroids and 7.6 ± 1.5 nm in straight bundles) (Supplementary Fig.13b). This indicates that ZapD not only connects FtsZ filaments laterally but spreads them apart, which could have important implications for the functionality of the Z ring.

These results point out the relevant role of the number of connections between filaments (driven by ZapD binding) in the crosslinking mechanism (Fig. 6). The bundles formed at the high ZapD concentrations assayed (up to four molar excess of ZapD to FtsZ) correspond to a binding saturation regime in which one ZapD binds two FtsZ molecules connecting filaments, which straightens their structure and arranges them into large, highly organized straight bundles, while a lower number of connections provides freedom to form toroidal structures.

This observation confirms that a certain number of ZapD-driven bonds are optimal for maintaining the preferential curvature of FtsZ filaments and enabling toroid assembly, establishing a structural dependence of assembled bundles on the number of ZapD-mediated bonds.

Dimerization of ZapD is essential to form organized high-order FtsZ structures

Our results suggest that ZapD dimers connect two FtsZ filaments, although the role of dimerization has not yet been experimentally established[42]. We therefore investigated whether the dimerization of ZapD was essential for assembling straight bundles and toroidal structures. To this end, we produced a ZapD mutant ("mZapD") by substituting three amino acids (R20, R116 and H140) involved in its dimerization by alanine, thus decreasing the stability of the dimerization interface (Supplementary Fig. 14a). mZapD can interact with unpolymerized FtsZ-GDP as evidenced by fluorescence anisotropy and FCS (Supplementary Fig. 14b and c). mZapD is still able to promote FtsZ bundle formation, showing a ~50% lower turbidity signal than for wild-type ZapD even at higher concentrations (Supplementary Fig. 14d). We also visualized these bundles by cryo-EM and observed the formation of thinner bundles (Supplementary Fig. 15b and c). However, toroidal structures and straight bundles were absent in these samples even at high concentrations of mZapD. This indicates that a stable dimerization interface is required to assemble complex ZapD-mediated structures (Supplementary Fig 15a).

These results demonstrated that dimerization of ZapD is essential to promote the assembly of organized high-order FtsZ structures such as toroids and straight bundles, highlighting the structural importance of stable ZapD-driven connections between filaments.

Discussion

In this study, we employed biochemical reconstitution and cryo-EM and cryo-ET to gain new insights into the structure and assembly of the bacterial divisome. In most bacteria, lateral crosslinking of filaments through the FtsZ-associated proteins (Zaps) is supposed to play a crucial role in assembling and stabilizing the Z ring, by however poorly understood mechanisms. To sight light on these, we studied the interaction between FtsZ and ZapD, one of the stabilizers of the division ring. We demonstrated that ZapD crosslinks FtsZ in solution into multilayered structures on a cellular scale. The three-dimensional architecture of this supramolecular structure consists of short, discontinuous FtsZ filaments connected laterally through ZapD molecules, as revealed by cryo-ET. In spite of the compositional simplicity of our reconstituted system, the structural organization of the FtsZ polymers by ZapD is compatible with the current model of the Z ring in the bacterial cell.

Our work demonstrates that ZapD can promote the assembly of FtsZ into higher-order toroidal structures in solution, formed by a meshwork of short, crosslinked filaments resembling those that form the division ring in bacterial cells[7,33,49,50,55,56]. These results are consistent with pre-curved FtsZ protofilaments, as suggested by the circular assemblies of FtsZ filaments flexibly attached to model membranes observed in several vitro reconstituted systems[57–59]. Besides, FtsZ can form ring-shaped structures with a 100-200 nm diameter on surfaces, as revealed by negative stain EM and AFM, which become even more prominent after FtsZ adsorption to lipid, carbon, or mica surfaces[12,13,60] or in the presence of molecular crowders such as

methylcellulose or polyvinyl alcohol[17]. Finally, cryo-EM of frozen-hydrated samples of highly concentrated (50 µM) FtsZ from B. subtilis with GMPCPP showed curved protofilaments that frequently coalesce into spirals or toroids, forming large aggregates[31].

The formation of toroidal structures is compatible with the robust persistence length and preferential curvature of the FtsZ filaments adapted by nature to form bacterial-sized ring-like structures[7,38]. ZapD helps to shape and stabilize the toroidal structure through crosslinking, spacing short FtsZ filaments further apart, from 5.9 ± 0.8 nm in the case of FtsZ-FtsZ interactions alone to 7.9 ± 2 nm in toroids and 7.6 ± 1.5 nm in straight bundles. Spacing filaments apart while crosslinking them by ZapD may facilitate a more dynamic organization, preventing rigid association and providing functional flexibility in bacterial cells.

We also demonstrated that ZapD-mediated FtsZ toroids recapitulate some of the structural features of the Z ring architecture *in vivo.* Based on super-resolution imaging and cryo-ET, the current model of the Z ring defines a somewhat discontinuous and heterogeneous structure composed of randomly overlapping filaments[33,49,55]. They arrange in a belt-like macromolecular entity containing nodes with a higher density of dispersed filaments confined to a toroidal zone around 80–100 nm wide (toroidal height) and a thickness of about 40–60 nm, located 13-16 nm below the inner membrane[33,39,49,51,55,56,61,62]. The toroidal structures promoted by ZapD showed dimensions in the same range (Fig. 2d and e, Supplementary Fig. 6b). However, the thickness and multilarity of the toroidal structures is significantly higher, likely due to the lack of other cellular components competing for the interaction with FtsZ. The Z ring model also suggests that FtsZ filaments are weakly associated with each other via protein factors such as Zaps and weak FtsZ-FtsZ interactions, which may play a crucial role in their functionality[2,7,31,32,63]. Here we have shown that one of the Zap proteins can stabilize and promote associations between neighboring FtsZ filaments. Studying macrostructures stabilized by natural crosslinkers is crucial for understanding the molecular function of the division machinery.

Structural characterization of the toroids by cryo-ET enabled us to resolve the overall structure and identify putative ZapD dimers crosslinking the filaments (Fig. 4). However, we could not obtain structural details of the ZapD connectors due to the heterogeneity and density of the toroids, with significant variability in the conformations of the connections between the filaments, formed in all directions. These observations align with the fact that the interaction of ZapD with FtsZ occurs via the FtsZ's central hub, which can offer additional spatial freedom to connect other filaments in various conformations, thus enabling different filament organizations and heterogeneity in the structure; moreover, they suggest that these crosslinkers act as modulators of ring structural dynamics, spacing filaments apart and allowing them to slide in an organized fashion[33,36,64,65]. The ability of FtsZ to treadmill directionally[58,59,66–68], and the parallel or antiparallel organization of short, transiently crosslinked filaments, are considered essential for Z ring functionality and force constriction[35–38,69]. Thus, Zap proteins can ensure correct filament placement and stabilization, consistent with the toroidal structure assembled by ZapD.

We have found that the amount of ZapD bound to FtsZ filaments has a marked impact on the structural organization of the final higher-order polymer. In this regard, at the lower ZapD concentration regime required for bundling (corresponding to equimolar mixtures of ZapD and FtsZ), the toroids were the most prominent structures containing one ZapD dimer per four to six FtsZ molecules. Higher ZapD concentration increased the ZapD binding density in the polymers to one ZapD dimer per two FtsZ molecules, which led to a reorganization of the polymer bundles to form straight structures crosslinking the FtsZ filaments predominantly,

structures never observed at lower ZapD concentrations (Fig. 5). The increase in the number of ZapD-FtsZ contacts may reduce the flexibility required to form the toroidal structure, forcing filaments to adopt a large, straight bundle conformation. We observed slight differences in the spacing between filaments (Supplementary Fig. 13b) and a larger range of distances between filaments in the toroids than in the straight bundles. The latter is reasonable, as ZapD is the molecule linking filaments in both structures. Still, the amount of bound ZapD is different, allowing higher variability in the spacing in certain areas where the number of connections is lower.

We therefore hypothesize that the assembly of functional, curved FtsZ macrostructures only occurs within a stoichiometric range of ZapD-FtsZ interactions, and that an increase in crosslinking at higher ZapD concentrations causes the FtsZ polymer to form rigid, less dynamic straight bundles (Fig. 6). Additionally, only a robust ZapD dimer can form FtsZ toroids and straight filaments, which indicates that certain binding strength is required to bundle the filaments and hold them in place. These observations, together with the high conformational variability found in ZapD connections, indicate that ZapD can modulate the behavior of the entire structure based on a concentration-dependent mechanism. This structural reorganization reflects the polymorphic nature of the assemblies formed by FtsZ, which would take a minor free energy perturbation to bring about significant changes in the geometry of the fibers due to modifications in environmental conditions[37,70].

Interestingly, the binding of ZapA (another member of the FtsZ-associated proteins family) to FtsZ in equimolar mixtures of ZapA and FtsZ resulted in the alignment and straightening of FtsZ filaments tethered to lipid bilayers by the proto-ring FtsA protein, as revealed by high-resolution fluorescence microscopy and quantitative image analysis (Caldas et al. 2019[71]). These structures corresponded to one ZapA tetramer per four FtsZ molecules in the polymer. Therefore, these straight parallel polymers, observed when ZapA is saturating the binding sites on the filament, resemble the straight bundles found in this study at the high ZapD concentration regime corresponding to ZapD binding saturation. How the state of association of ZapA and ZapD (tetramers and dimers, respectively) and membrane tethering determine the predominant structure formed in both systems remained to be analyzed under well-controlled conditions of protein compositions.

In summary, this work expands our current understanding of the structural organization and filament crosslinking of FtsZ polymers by the action of ZapD. The finding that ring morphology depends on the binding stoichiometry between FtsZ and the crosslinking ZapD provides valuable information to be combined with reconstitution assays in membrane systems currently underway to decipher how the FtsZ associated proteins are responsible for coordinating and maintaining the formation of the division ring. Moreover, our results will have implications for understanding the remodeling of other cytoskeletal polymer networks involved in essential cellular processes, such as cell motility or morphogenesis. Traditionally, the general assumption is that processes consuming chemical energy, such as the action of molecular motors, are the main drivers of dynamic filament remodeling of polymer networks. However, increasing evidence points to alternative cytoskeletal network remodeling mechanisms that do not rely on chemical energy consumption as those in which entropic forces act through diffusible crosslinkers, similar to ZapD and FtsZ polymers. These energy-independent mechanisms of polymer network remodeling via diffusible protein cross-linkers might also be relevant to optimize conditions for reverse engineering the division ring for improved force generation in minimal reconstituted systems for autonomous cell division.

Methods

Protein purification: ZapD protein has been overproduced and purified following the procedure previously described in[21] with some modifications. The bacterial strain was an *E. coli* BL21 (DE3) transformed with pET28b-h10-smt3-ZapD fusion plasmid[21]. The cells were sonicated for 6-8 cycles of 20 secs and centrifuged at 40.000 rpm in MLA 80 rotor (Beckman coulter) for 45 min. The protein was eluted by chromatography in 5-ml HisTrap (GE Healthcare) and digested with Smt3-specific protease Ulp1 (SUMO protease encoded in Rosetta pTB145), at 1:1 molar relation. Digestion proceeded for two dialysis of 1 hour at 4°C to avoid protein precipitation. ZapD and His-Smt3 were separated by chromatography in 5-ml HisTrap (GE Healthcare), then the protein was eluted in a 5-ml HiTrap Desalting column (Healtcare) to eliminate completely possible traces of free phosphates in the buffer. Final concentration of ZapD was determined by absorbance at 280 nm using an extinction coefficient (ε) of 25230 M^{-1} cm^{-1} and ZapD purity was checked by SDS-polyacrylamide gel electrophoresis. Protein fractions were frozen in buffer 50 mM KCL, 50 mM Tris-CL, 10 mM $MgCl_2$, 0.2 mM DTT and 2% glycerol. ZapD mutant (mZapD) was purified following the same procedure using the corresponding plasmid. *E. coli* FtsZ was overproduced and purified following the calcium precipitation method described previously[52]. Briefly, E. coli BL21 (DE3) pLysS cells were transformed with pET11b-FtsZ, grown in LB medium and selected with Ampicillin 100 µg/mL. After induction and growth, the pellet was resuspended in PEM buffer (50 mM PIPES-NaOH, pH 6.5, 5 mM $MgCl_2$, 1 mM EDTA) and disrupted using a tip sonicator for 3-4 cycles. The lysate was then separated by centrifugation for 30 min at 20,000 x g at 4 °C, and the supernatant was mixed with 1 mM GTP, 20 mM $CaCl_2$ and incubated at 30 ºC for 15 min to induce FtsZ polymerization and bundling. Subsequently, the FtsZ bundles were pelleted by centrifugation for 15 min at 20,000 x g at 4 °C, and the pellet was resuspended in PEM buffer and centrifuged again for 15 min at 20,000 x g, 4 °C, collecting the supernatant. Precipitation and resuspension steps were repeated to improve the purification. The buffer was then exchanged using an Amicon Ultra-0.5 centrifugal filter unit 50 kDa (Merck KGaA). FtsZ purity was checked by SDS-polyacrylamide gel electrophoresis and concentration was determined by absorbance at 280 nm using an extinction coefficient (ε) of 14000 M^{-1} cm^{-1} [52]. Protein solutions were aliquoted, frozen in liquid nitrogen, and stored at -80 °C until further use.

Plasmid Design and Molecular Cloning: To generate the ZapD mutant (mZapD), seamless cloning method was used according to the provider's protocol (ThermoFisher Scientific /Invitrogen GeneArt™ Seamless Cloning and Assembly Enzyme Mix (A14606)) using the plasmid pET28b-h10-smt3-ZapD and the primers listed in (Supplementary Table 1). All enzymes for cloning were from Thermo Fisher Scientific (Waltham, MA, USA). Briefly, DNA fragments were amplified with Phusion High-Fidelity DNA Polymerase andorigo primers (Sigma–Aldrich, St. Louis, MO, USA). Then, PCR products were treated with DpnI and combined using GeneArt Seamless Cloning and Assembly Enzyme Mix. The plasmid was propagated in E. coli OneShot TOP10 (Thermo Fisher Scientific) and purified using NucleoBond Xtra Midi kit (Macherey-Nagel GmbH, Duren, Germany). Directed site mutagenesis was made by substituting three amino acids in the ZapD sequence by Alanine (R20, R116, H140). The plasmid was then verified using Sanger Sequencing Service (Microsynth AG, Balgach, Switzerland).

Protein labelling: Covalent labelling of FtsZ with Alexa 488 the amino groups of N-terminal amino acid residue with Alexa Fluor 488 carboxylic acid succinimidyl ester dye following the procedure previously described[16]. ZapD and mZapD were labelled with ATTO-647N carboxylic

acid succinimidyl ester dye in the amino group. Before the reaction, ZapD was dialyzed in 20 mM HEPES, 50 mM KCl, 5 mM $MgCl_2$, pH 7.5 and the probe was dissolved in Dimethylsulfoxide (DMSO). The reaction was allowed to proceed for 35-60 min at RT and stopped with 10 % Tris-HCl 1 M. The free dye was separated from labelled protein by a Hi-TRAP Desalting column (GE Healthcare). The final degree of labelling of FtsZ and ZapD was calculated from the molar absorption coefficients of the protein and the dye. It was around 0.5 moles of probe per mole of FtsZ and around 0.3/0.4 moles of dye per mole of ZapD.

Analytical ultracentrifugation; sedimentation velocity (SV) and sedimentation equilibrium (SE): Sedimentation velocity assays were performed to detect the homogeneity and association state of individual proteins and the stoichiometry of the formed protein-protein complexes. In brief, the experiments were carried out at 43-48 Krpm in an Optima XL-I analytical ultracentrifuge, equipped with UV–VIS absorbance and Raleigh interference detection systems. The sedimentation coefficient distributions were calculated by least-squares boundary modeling of sedimentation velocity data using the c(s) method[72] as implemented in the SEDFIT program. The s-values of the present species were corrected to standard conditions (pure water at 20ºC, and extrapolated to infinite dilution) to obtain the corresponding standard s-values (s20,w) using the program SEDNTERP[73]. Multi-signal sedimentation velocity (MSSV) data were globally analyzed by SEDPHAT software[74] using the "multi-wavelength discrete/continuous distribution analysis" model, to determine the spectral and diffusion deconvoluted sedimentation coefficient distributions, ck(s), from which the stoichiometry of protein complexes can be derived[75]. Sedimentation equilibrium of ZapD was carried out to confirm the association state of the protein in the same experimental conditions and concentration range tested by sedimentation velocity (2-30 µM). Short columns (100 µL) SE experiments were carried out at 14000 and 10000 rpm. Weight-average buoyant molecular weights were obtained by fitting a single-species model to the experimental data using the HeteroAnalysis program[76], once corrected for temperature and buffer composition with the program SEDNTERP[73].

Turbidity assay: Turbidity of protein samples was collected by measuring the absorbance at 350 nm in a TECAN plate reader (Tecan Group Ltd., Mannedorf, Switzerland). All samples reached a final volume of 50 µL in a 364-Well Flat-Bottom Microplate (UV-Star, Greiner Bio-One GmbH) before measuring the absorbance. Different concentrations of FtsZ and ZapD were premixed in the well-plate and measured before addition of GTP to extract subsequently the individual blank values. Concentrations of FtsZ and ZapD varied from 0 to 80 µM and buffer conditions are specified in each graph and the caption of the figures ranging from 50 to 500 mM KCl, 6 to 8 pH, always supplemented with 50 mM Tris-Cl and 5 mM $MgCl_2$. Manual mixing was performed after addition of GTP and orbital oscillations for 5 sec in the TECAN were made prior to any measurement to avoid sedimentation of the samples. Time measurements were taken as specified in each condition. Reported values are the average of 3-12 independent measurements ± Standard deviation.

GTPase activity of FtsZ: GTPase activity of FtsZ was measured by quantification of the inorganic phosphate with a colorimetric assay (BIOMOL GREENÒ kit from ENZO life sciences) for two minutes. 5 µM FtsZ was used in our standard buffer (5 mM $MgCl_2$, 50 mM Tris-HCl, 50 mM KCl, pH 7) or buffers at higher KCl concentrations (50-500 mM KCl) and polymerization was triggered by 1 mM GTP. ZapD was added at different concentrations and premixed with FtsZ before addition of GTP. 13 µL fractions were added to a 96-Well Flat-Bottom Microplate (UV-Star, Greiner Bio-One GmbH) every 20 sec after addition of GTP and mixed with the

Reaction buffer reaching 50 µL and 100 µL of BIOMOL GREEN reagent, to stop the reaction. After stopping the reaction, samples were incubated for 10 min at RT and the absorbance was measured at 620 nm in a Varioskan Flash plate reader (Thermo Fisher Scientific, MA, USA). Concentrations of inorganic Phosphate were calculated from a phosphate standard curve, while the GTPase activity reaction rate (V, mol P/mol FtsZ/ min) was determined from the slope of the linear part of phosphate accumulation curves.

FtsZ sedimentation assay: Purified ZapD (1-30 µM) was added to purified FtsZ (5 µM) in the working buffer (50 mM KCl, 50 mM Tris-HCl, 5 mM $MgCl_2$), and GDP or GTP (1 mM) was added last to trigger FtsZ polymerization. The reaction mixtures with a final volume of 100 µl were processed at room temperature and centrifuged at low speed (10.000 rcf) using a table top centrifuge. At that point, 90 µl of supernatant was carefully collected and loaded in clean tubes with 1x loading dye. The rest of the supernatant was discarded and the pellets were resuspended in the original reaction volume buffer plus 1× loading dye (final concentration). The supernatants (10 µl) and pellets (10 µl) were resolved in a SDS-PAGE gel. The amount of ZapD and FtsZ were estimated by image analysis using ImageJ.

Preparation of EM grids. Cryo-EM grids were plunge frozen with a Vitrobot Mk.IV (Thermo Fischer Scientific) using 3 µL of the samples applied to previously glow discharged R 2/1 Holey Carbon Cu 200 mesh EM grids (Quantifoil). Samples were 10 µM FtsZ with or without ZapD or mZapD at different concentrations specified in each case (0 – 60 µM). Proteins were mixed in our working buffer containing 50 mM, 5 mM $MgCl_2$, 50 mM Tris-HCl, pH 7. Samples were incubated for 2 minutes after the addition of 1 mM GTP to trigger polymerization. The Vitrobot was set to 4° C, 100% humidity, blot time 3 s, blot force 3. Whatman no. 1 filter paper was used for blotting and liquid ethane kept at liquid nitrogen temperatures was used as a cryogen for vitrification.

Cryo-EM and cryo-ET. Cryo-EM data was acquired on two microscopes as follows. Cryo-EM micrographs were acquired within SerialEM[77] on a Talos Arctica transmission electron microscope (Thermo Fisher Scientific) operated at 200 kV, equipped with a Falcon III (Thermo Fisher Scientific) direct electron detector operated in integrating mode. Images were recorded at 73,000x magnification (pixel size 1.997 Å) and 92,000x magnification (pixel size 1.612 Å) at -2.5 µm to -5 µm target defocus with an approximate total electron dose of 60 electrons / $Å^2$.

Cryo-EM micrographs and Cryo-ET tilt series were acquired within SerialEM on a G2 Titan Krios transmission electron microscope (Thermo Fisher Scientific) operated at 300 kV, equipped with a FEG, post-column energy filter (Gatan) and a K3 camera (Gatan) operated in electron counting mode. Micrographs were recorded at 42,000x magnification (pixel size 2.154 Å) at -5 µm target defocus with an approximate total electron dose of 60 electrons / $Å^2$. Tilt series were recorded at 42,000x magnification (pixel size 2.154 Å) at -5 µm target defocus with an approximate total electron dose of 100-140 electrons / $Å^2$. Acquisition was performed using a dose-symmetric tilt scheme, a tilt range of +/-60°, an angular increment of 2°.

Tomogram reconstruction: Tilt series preprocessing was performed using the TOMOMAN package (https://github.com/williamnwan/TOMOMAN). In brief, MotionCor2[78] was used to align individual frames, followed by cumulative dose-weighting using an exposure-dependent attenuation function, as described in[79]. Dose-weighted tilt series were aligned using IMOD[80] either by employing gold fiducials (if available) or by patch-tracking, and binned tomograms (pixel size 8.616 Å) were generated using weighted back-projection. Stacks were split into odd

and even frames to generate half-set tomograms which were used for training and subsequent denoising in cryoCARE[81].

Denoised tomograms were directly employed for segmentation of the toroids, straight bundles and individual filaments by cropping an area of interest and displaying the volume as isosurface in USCF ChimeraX[82]. To highlight connections between filaments, the respective parts were cropped from the volume using the Volume Eraser tool in USCF Chimera[83].

All micrographs and slices through tomograms were visualized using IMOD. Isosurface renderings of toroids, straight bundles and individual filaments were displayed using USCF ChimeraX and USCF Chimera.

Fluorescence anisotropy: Anisotropy measurements were performed using a TECAN plate reader (Tecan Group Ltd., Mannedorf, Switzerland). Excitation and emission wavelengths were 625 nm and 680 nm, respectively. ZapD or mZapD labelled with ATTO 647N were used as fluorescence tracer with a final concentration of 150 nM of ATTO-647N and supplemented with unlabeled ZapD reaching a concentration of 5 µM. FtsZ was added at increasing concentrations to analyze their interaction. Binding affinities (apparent K_D) were determined by fitting the Hill equation to the normalized anisotropy data. Each condition was measured in three independent samples.

Fluorescence correlation spectroscopy (FCS): FCS measurements were performed using a PicoQuant MicroTime200 system equipped with an Olympus 60x, NA1.2 UPlanApo water immersion objective. A pulsed 636 nm diode laser was used to excite fluorescence of Atto647N-labelled ZapD, mZapD or free Atto647N carboxylate (for calibration). Three measurements of 60 s each were performed per sample at room temperature (21°C), and three samples per condition were measured. The repetition rate of the pulsed laser was 26.7 MHz, and the average power was 1 µW at the objective back pupil. Fluorescence was collected through the same objective, spatially filtered through a 50 µm diameter pinhole, and spectrally filtered through a 690/70 nm bandpass filter before being split by a neutral beam splitter onto two avalanche photodiodes (Excelitas SPCM-AQRH-14-TR). Photon count events were digitized using a PicoQuant TimeHarp 260 Nano TCSPC card. Time-correlated single photon counting information was used for monitoring data quality during measurements, but not in further analysis. As especially in samples with FtsZ ZapD, and GTP present simultaneously we occasionally saw large, bright particles that are difficult to treat in FCS analysis, data was subjected to a burst removal algorithm similar to Margineanu et al. [84] and only “non-burst” data was used in correlation analysis to obtain statistics representative of the large number of small oligomer particles, ignoring rare large ones. Cross-correlation functions of the two detectors were calculated and fitted with a standard model for three-dimensional diffusion in with rapid dye blinking:

$$G(\tau) = G_0 \left[\frac{1 - F_B + F_B e^{-\frac{\tau}{\tau_B}}}{1 - F_B} \right] \frac{1}{1 + \frac{\tau}{\tau_d}} \sqrt{\frac{1}{1 + \frac{\tau}{S^2 \tau_d}}}$$

With amplitude G_0, diffusion time τ_d, point spread function aspect ratio S, and blinking parameters F_B and τ_B. Custom software was written in Python for burst removal, correlation, and fitting, based on tttrlib 0.0.19 (https://github.com/Fluorescence-Tools/tttrlib). The software is in ongoing development, and available upon request.

Image analysis: Electron microscopy images were processed and analyzed using IMOD and ImageJ. The dimensions of the toroidal structures, FtsZ bundles and distances between filaments were manually measured using ImageJ and IMOD. Distances were plotted as histograms using Origin (OriginPro, Version *2019b*. OriginLab Corporation, Northampton, MA, USA.). For each toroid analyzed (n = 67) the inner and outer diameter were measured collecting the major and minor distance in each case. The circularity of the toroid was the result of the division between the minor diameter divided by major diameter for each toroid. The height of the FtsZ toroid was manually measured from the tomograms, collecting 4 measurements per toroid to assure a correct representation of the size (n = 17). For the distances between filaments, they were also manually measured by using IMOD. Each measurement represents only one FtsZ double filament or one FtsZ-ZapD double filament, however, the same bundle could be measured more than once as they are composed for multiple filaments. The measurements were collected from >3 independent samples. The distances between ZapDs connecting two FtsZ filaments were measured following the same methodology. The mean value and standard deviation of different datasets were calculated and added to the figures together with the n used for each case.

Acknowledgements

We thank Daniel Bollschweiller (MPIB cryo-EM facility) and Rafael Nuñez (CIB-CSIC imaging facility) for their help with the cryo-EM experiments. We also thank the MPIB core facility for assistance in protein purification, Michaela Schaper for plasmid cloning, Sigrid Bauer for lipid preparation and Noelia Ropero, Katharina Nakel and Kerstin Andersson for protein purification. We are also grateful to Miguel Robles-Ramos, Ana Raso, Hiromune Eto, Cristina Capitanio, Pedro Weickert, Kareem Al-Nahas, Yusuf Qutbuddin, Silvia Zorrilla, Henri Franquelim, Diego Ramirez and Daniela Garcia-Soriano for helpful discussions and fruitful input in this work. This work was funded by the Max Planck-Bristol Centre for Minimal Biology (A.M.-S.), the Deutsche Forschungsgemeinschaft (P.S.), the French Agence Nationale de la Recherche (ANR) (J.S. and M.Ja.), the Deutsche Forschungsgemeinschaft (DFG) call ANR-DFG 2020 NLE through the grant JA-3038/2-1 (M. Ja.), the Germany´s Excellence Strategy – EXC-2094 – 390783311 (J.-H.K) and the Spanish Government through Grants PID2019-104544GB-I00 and PID2022_136951NB-I00 (G.R.). M.S.-S. was supported by European Social Fund through Grant PTA2020-018219-I. J.R.L.-O and M S.-S. acknowledge support from the Molecular Interactions Facility at the CIB Margarita Salas-CSIC. A.M.-S and J.-H.K. are part of IMPRS-LS, J.-H.K. is also a CeNS Center for NanoScience associate.

Author contributions

Designing of research: A.M.-S., M.Ji., M.Ja., P.S., and G.R. Performing of research: A.M.-S, J.S., L.B., T.S., M.S.-S., M.Ji., C.A. and J.R.L.-OData analysis: A.M.-S, J.S., T.S., M. Ja., M.Ji., C.A., J.R.L.-O, and G.R. Manuscript writing: A.M.-S (first draft); A.M.-S., M.Ja. P.S., and G.R. (final version); all authors revised and edited the manuscript, read the final version and approved to be published.

References

1. Levin, P. A. & Janakiraman, A. Localization, Assembly, and Activation of the Escherichia coli Cell Division Machinery. *EcoSal Plus* **9**, (2021).

2. Du, S. & Lutkenhaus, J. At the Heart of Bacterial Cytokinesis: The Z Ring. *Trends Microbiol.* **27**, 781–791 (2019).

3. Attaibi, M. & Den Blaauwen, T. An Updated Model of the Divisome: Regulation of the Septal Peptidoglycan Synthesis Machinery by the Divisome. *Int. J. Mol. Sci.* (2022) doi:10.3390/ijms23073537.

4. Nogales, E., Downing, K. H., Amos, L. A. & Löwe, J. Tubulin and FtsZ form a distinct family of GTPases. *Nat. Struct. Biol. 1998 56* **5**, 451–458 (1998).

5. De Boer, P., Crossley, R. & Rothfield, L. The essential bacterial cell-division protein FtsZ is a GTPase. *Nat. 1992 3596392* **359**, 254–256 (1992).

6. Addinall, S. G. & Lutkenhaus, J. FtsA is localized to the septum in an FtsZ-dependent manner. *J. Bacteriol.* **178**, 7167–7172 (1996).

7. McQuillen, R. & Xiao, J. Insights into the Structure, Function, and Dynamics of the Bacterial Cytokinetic FtsZ-Ring. *Annu. Rev. Biophys.* **49**, 309–341 (2020).

8. Wang, M., Chao Fang, ·, Ma, B., Luo, X. & Hou, Z. Regulation of cytokinesis: FtsZ and its accessory proteins. *Curr. Genet.* **66**, 43–49 (2020).

9. Small, E. & Addinall, S. G. Dynamic FtsZ polymerization is sensitive to the GTP to GDP ratio and can be maintained at steady state using a GTP-regeneration system. *Microbiology* **149**, 2235–2242 (2003).

10. Erickson, H. P., Taylor, D. W., Taylor, K. A. & Bramhill, D. Bacterial cell division protein FtsZ assembles into protofilament sheets and minirings, structural homologs of tubulin polymers. *Proc. Natl. Acad. Sci. U. S. A.* **93**, 519–523 (1996).

11. Lu, C., Reedy, M. & Erickson, H. P. Straight and curved conformations of FtsZ are regulated by GTP hydrolysis. *J. Bacteriol.* **182**, 164–170 (2000).

12. Mingorance, J. *et al.* Visualization of single Escherichia coli FtsZ filament dynamics with atomic force microscopy. *J. Biol. Chem.* **280**, 20909–20914 (2005).

13. Huecas, S. *et al.* The interactions of cell division protein FtsZ with guanine nucleotides. *J. Biol. Chem.* **282**, 37515–37528 (2007).

14. Mukherjee, A. & Lutkenhaus, J. Analysis of FtsZ assembly by light scattering and determination of the role of divalent metal cations. *J. Bacteriol.* **181**, 823–832 (1999).

15. Löwe, J. & Amos, L. A. Tubulin-like protofilaments in Ca2+-induced FtsZ sheets. *EMBO J.* **18**, 2364–2371 (1999).

16. González, J. M. *et al.* Essential cell division protein FtsZ assembles into one monomer-thick ribbons under conditions resembling the crowded intracellular environment. *J. Biol. Chem.* **278**, 37664–37671 (2003).

17. Popp, D., Iwasa, M., Narita, A., Erickson, H. P. & Maéda, Y. FtsZ Condensates: An In Vitro Electron Microscopy Study. *Biopolymers* **91**, 340–350 (2009).

18. Ma, X. & Margolin, W. Genetic and Functional Analyses of the Conserved C-Terminal Core Domain of Escherichia coli FtsZ. *J. Bacteriol.* **181**, 7531–7544 (1999).

19. Hale, C. A. & De Boer, P. A. J. J. Direct binding of FtsZ to ZipA, an essential component of the septal ring structure that mediates cell division in E. coli. *Cell* **88**, 175–185 (1997).

20. Wang, X., Huang, J., Mukherjee, A., Cao, C. & Lutkenhaus, J. Analysis of the

interaction of FtsZ with itself, GTP, and FtsA. *J. Bacteriol.* **179**, 5551–5559 (1997).

21. Durand-Heredia, J., Rivkin, E., Fan, G., Morales, J. & Janakiraman, A. Identification of ZapD as a cell division factor that promotes the assembly of FtsZ in Escherichia coli. *J. Bacteriol.* **194**, 3189–3198 (2012).

22. Huang, K.-H. H., Durand-Heredia, J. & Janakiraman, A. FtsZ ring stability: Of bundles, tubules, crosslinks, and curves. *J. Bacteriol.* **195**, 1859–1868 (2013).

23. Durand-Heredia, J. M., Yu, H. H., De Carlo, S., Lesser, C. F. & Janakiraman, A. Identification and characterization of ZapC, a stabilizer of the FtsZ ring in Escherichia coli. *J. Bacteriol.* **193**, 1405–1413 (2011).

24. Ebersbach, G., Galli, E., Møller-Jensen, J., Löwe, J. & Gerdes, K. Novel coiled-coil cell division factor ZapB stimulates Z ring assembly and cell division. *Mol. Microbiol.* **68**, 720–735 (2008).

25. Gueiros-Filho, F. J. & Losick, R. A widely conserved bacterial cell division protein that promotes assembly of the tubulin-like protein FtsZ. *Genes Dev.* **16**, 2544–2556 (2002).

26. de Boer, P. A. J., Crossley, R. E. & Rothfield, L. I. A division inhibitor and a topological specificity factor coded for by the minicell locus determine proper placement of the division septum in E. coli. *Cell* **56**, 641–649 (1989).

27. Tonthat, N. K. *et al.* Molecular mechanism by which the nucleoid occlusion factor, SlmA, keeps cytokinesis in check. *EMBO J.* **30**, 154–164 (2011).

28. Ortiz, C., Natale, P., Cueto, L. & Vicente, M. The keepers of the ring: regulators of FtsZ assembly. *FEMS Microbiol. Rev.* **040**, 57–67 (2016).

29. Buske, P. J., Mittal, A., Pappu, R. V. & Levin, P. A. An intrinsically disordered linker plays a critical role in bacterial cell division. *Semin. Cell Dev. Biol.* **37**, 3–10 (2015).

30. Buske, P. J. & Levin, P. A. Extreme C terminus of bacterial cytoskeletal protein FtsZ plays fundamental role in assembly independent of modulatory proteins. *J. Biol. Chem.* **287**, 10945–10957 (2012).

31. Huecas, S. *et al.* Self-Organization of FtsZ Polymers in Solution Reveals Spacer Role of the Disordered C-Terminal Tail. *Biophys. J.* **113**, 1831–1844 (2017).

32. Sundararajan, K. & Goley, E. D. The intrinsically disordered C-terminal linker of FtsZ regulates protofilament dynamics and superstructure in vitro. *J. Biol. Chem.* **292**, 20509–20527 (2017).

33. Szwedziak, P., Wang, Q., Bharat, T. A. M. M., Tsim, M. & Löwe, J. Architecture of the ring formed by the tubulin homologue FtsZ in bacterial cell division. *Elife* **3**, e04601 (2014).

34. Söderström, B., Daniel, · & Daley, O. The bacterial divisome: more than a ring? *Curr Genet* **63**, 161–164 (2017).

35. Erickson, H. P., Anderson, D. E. & Osawa, M. FtsZ in Bacterial Cytokinesis: Cytoskeleton and Force Generator All in One. *Microbiol. Mol. Biol. Rev.* **74**, 504–528 (2010).

36. Nguyen, L. T., Oikonomou, C. M. & Jensen, G. J. Simulations of Proposed Mechanisms of FtsZ-Driven Cell Constriction. *J. Bacteriol.* **203**, (2021).

37. Mateos-Gil, P., Tarazona, P., ´ Elez, M. V & Vélez, M. Bacterial cell division: modeling FtsZ assembly and force generation from single filament experimental data. *FEMS Microbiol. Rev.* **039**, 73–87 (2019).

38. Erickson, H. P. & Osawa, M. FtsZ Constriction Force-Curved Protofilaments Bending Membranes. *Subcell. Biochem.* **84**, (2017).

39. Buss, J. *et al.* In vivo organization of the FtsZ-ring by ZapA and ZapB revealed by quantitative super-resolution microscopy. *Mol. Microbiol.* **89**, 1099–1120 (2013).

40. Hale, C. A. *et al.* Identification of Escherichia coli ZapC (YcbW) as a component of the division apparatus that binds and bundles FtsZ polymers. *J. Bacteriol.* **193**, 1393–1404 (2011).

41. Schumacher, M. A., Zeng, W., Huang, K. H., Tchorzewski, L. & Janakiraman, A. Structural and functional analyses reveal insights into the molecular properties of the Escherichia coli Z ring stabilizing protein, ZapC. *J. Biol. Chem.* **291**, 2485–2498 (2016).

42. Schumacher, M. A., Huang, K. H., Zeng, W. & Janakiraman, A. Structure of the z ring-associated protein, zapd, bound to the c-terminal domain of the tubulin-like protein, ftsz, suggests mechanism of z ring stabilization through ftsz cross-linking. *J. Biol. Chem.* **292**, 3740–3750 (2017).

43. Pazos, M., Natale, P., Margolin, W. & Vicente, M. Interactions among the early Escherichia coli divisome proteins revealed by bimolecular fluorescence complementation. *Environ. Microbiol.* **15**, 3282–3291 (2013).

44. Marteyn, B. S. *et al.* ZapE Is a Novel Cell Division Protein Interacting with FtsZ and Modulating the Z-Ring Dynamics. *MBio* (2014) doi:10.1128/mBio.00022-14.

45. Bailey, M. W., Bisicchia, P., Warren, B. T., Sherratt, D. J. & Männik, J. Evidence for Divisome Localization Mechanisms Independent of the Min System and SlmA in Escherichia coli. *PLOS Genet.* **10**, e1004504 (2014).

46. Huang, K. H., Mychack, A., Tchorzewski, L. & Janakiraman, A. Characterization of the FtsZ C-Terminal variable (CTV) Region in Z-Ring assembly and interaction with the Z-Ring stabilizer ZapD in E. coli cytokinesis. *PLoS One* **11**, 1–24 (2016).

47. Choi, H., Min, K., Mikami, B., Yoon, H. J. & Lee, H. H. Structural and Biochemical Studies Reveal a Putative FtsZ Recognition Site on the Z-ring Stabilizer ZapD. *Mol. Cells* **39**, 814–820 (2016).

48. Roach, E. J. *et al.* Structure and mutational analyses of Escherichia coli ZapD reveal charged residues involved in FtsZ filament bundling. *J. Bacteriol.* **198**, 1683–1693 (2016).

49. Fu, G. *et al.* In Vivo Structure of the E. coli FtsZ-ring Revealed by Photoactivated Localization Microscopy (PALM). *PLoS One* **5**, e12680 (2010).

50. Li, Z., Trimble, M. J., Brun, Y. V. & Jensen, G. J. The structure of FtsZ filaments in vivo suggests a force-generating role in cell division. *EMBO J.* **26**, 4694–4708 (2007).

51. Lyu, Z., Coltharp, C., Yang, X. & Xiao, J. Influence of FtsZ GTPase activity and concentration on nanoscale Z-ring structure in vivo revealed by three-dimensional Superresolution imaging. *Biopolymers* **105**, 725–734 (2016).

52. Rivas, G. *et al.* Magnesium-induced linear self-association of the FtsZ bacterial cell division protein monomer. The primary steps for FtsZ assembly. *J. Biol. Chem.* (2000) doi:10.1074/jbc.275.16.11740.

53. Kourkoutis, L. F., Plitzko, J. M. & Baumeister, W. Electron Microscopy of Biological Materials at the Nanometer Scale. *https://doi.org/10.1146/annurev-matsci-070511-155004* **42**, 33–58 (2012).

54. Trueba, F. J. & Woldringh, C. L. 1. Yao Q, Jewett AI, Chang Y-W, Oikonomou CM,

Beeby M, Iancu C V, et al. Short FtsZ filaments can drive asymmetric cell envelope constriction at the onset of bacterial cytokinesis. EMBO J. 2017;36: 1577–1589. doi:10.15252/EMBJ.201696235Changes in cell dia. *J. Bacteriol.* **142**, 869–878 (1980).

55. Rowlett, V. W. & Margolin, W. 3D-SIM Super-resolution of FtsZ and Its Membrane Tethers in Escherichia coli Cells. *Biophys. J.* **107**, L17–L20 (2014).

56. Coltharp, C., Buss, J., Plumer, T. M. & Xiao, J. Defining the rate-limiting processes of bacterial cytokinesis. *Proc. Natl. Acad. Sci. U. S. A.* **113**, E1044–E1053 (2016).

57. Boutte, C. C., Srinivasan, R., Sass, P. & Vélez, M. How Does the Spatial Confinement of FtsZ to a Membrane Surface Affect Its Polymerization Properties and Function? *Front. Microbiol.* **13**, 757711 (2022).

58. Loose, M. & Mitchison, T. J. The bacterial cell division proteins FtsA and FtsZ self-organize into dynamic cytoskeletal patterns. *Nat. Cell Biol.* **16**, (2014).

59. Ramirez-Diaz, D. A. *et al.* Treadmilling analysis reveals new insights into dynamic FtsZ ring architecture. *PLOS Biol.* **16**, e2004845 (2018).

60. González, J. M. *et al.* Cooperative behavior of Escherichia coli cell-division protein FtsZ assembly involves the preferential cyclization of long single-stranded fibrils. *Proc. Natl. Acad. Sci.* **102**, 1895–1900 (2005).

61. Holden, S. J. *et al.* High throughput 3D super-resolution microscopy reveals Caulobacter crescentus in vivo Z-ring organization. *Proc. Natl. Acad. Sci. U. S. A.* **111**, 4566–4571 (2014).

62. Szwedziak, P. & Ghosal, D. FtsZ-ring architecture and its control by MinCD. *Subcell. Biochem.* **84**, 213–244 (2017).

63. Haeusser, D. P., Rowlett, V. W. & Margolin, W. A mutation in Escherichia coli ftsZ bypasses the requirement for the essential division gene zipA and confers resistance to FtsZ assembly inhibitors by stabilizing protofilament bundling. *Mol. Microbiol.* **97**, 988–1005 (2015).

64. Lan, G., Daniels, B. R., Dobrowsky, T. M., Wirtz, D. & Sun, S. X. Condensation of FtsZ filaments can drive bacterial cell division. *Proc. Natl. Acad. Sci. U. S. A.* **106**, 121–126 (2009).

65. Hörger, I., Velasco, E., Rivas, G., Vélez, M. & Tarazona, P. FtsZ Bacterial Cytoskeletal Polymers on Curved Surfaces: The Importance of Lateral Interactions. *Biophys. J.* **94**, L81–L83 (2008).

66. Yang, X. *et al.* GTPase activity-coupled treadmilling of the bacterial tubulin FtsZ organizes septal cell wall synthesis. *Science (80-.).* **355**, 744–747 (2017).

67. Bisson-Filho, A. W. *et al.* Treadmilling by FtsZ filaments drives peptidoglycan synthesis and bacterial cell division. *Science (80-.).* **355**, 739–743 (2017).

68. Whitley, K. D. *et al.* FtsZ treadmilling is essential for Z-ring condensation and septal constriction initiation in Bacillus subtilis cell division. *Nat. Commun.* **12**, 1–13 (2021).

69. Coltharp, C. & Xiao, J. Beyond force generation: Why is a dynamic ring of FtsZ polymers essential for bacterial cytokinesis? *BioEssays* **39**, 1–11 (2017).

70. Monterroso, B., Alfonso, C., Zorrilla, S. & Rivas, G. *Combined analytical ultracentrifugation, light scattering and fluorescence spectroscopy studies on the functional associations of the bacterial division FtsZ protein*. *Methods* vol. 59 349–362 (Academic Press Inc., 2013).

71. Caldas, P. *et al.* Cooperative ordering of treadmilling filaments in cytoskeletal networks

of FtsZ and its crosslinker ZapA. *Nat. Commun. 2019 101* **10**, 1–13 (2019).

72. Schuck, P. Size-distribution analysis of macromolecules by sedimentation velocity ultracentrifugation and lamm equation modeling. *Biophys. J.* **78**, 1606–1619 (2000).

73. Laue, T. M., Shah, B. D., Ridgeway, T. M. & Pelletier, S. L. *Analytical ultracentrifugation in biochemistry and polymer science*. *Analytical ultracentrifugation in biochemistry and polymer science* (Royal Society of Chemistry, 1992).

74. Schuck, P. On the analysis of protein self-association by sedimentation velocity analytical ultracentrifugation. *Anal. Biochem.* **320**, 104–124 (2003).

75. Balbo, A. *et al.* Studying multiprotein complexes by multisignal sedimentation velocity analytical ultracentrifugation. *Proc. Natl. Acad. Sci. U. S. A.* **102**, 81–86 (2005).

76. Cole, J. L. Analysis of Heterogeneous Interactions. *Methods Enzymol.* **384**, 212–232 (2004).

77. Mastronarde, D. N. Automated electron microscope tomography using robust prediction of specimen movements. *J. Struct. Biol.* **152**, 36–51 (2005).

78. Zheng, S. Q. *et al.* MotionCor2: anisotropic correction of beam-induced motion for improved cryo-electron microscopy. *Nat. Methods 2017 144* **14**, 331–332 (2017).

79. Schur, F. K. M. *et al.* An atomic model of HIV-1 capsid-SP1 reveals structures regulating assembly and maturation. *Science (80-.).* **353**, 506–508 (2016).

80. Kremer, J. R., Mastronarde, D. N. & McIntosh, J. R. Computer Visualization of Three-Dimensional Image Data Using IMOD. *J. Struct. Biol.* **116**, 71–76 (1996).

81. Buchholz, T. O., Jordan, M., Pigino, G. & Jug, F. Cryo-CARE: Content-aware image restoration for cryo-transmission electron microscopy data. *Proc. - Int. Symp. Biomed. Imaging* **2019**-**April**, 502–506 (2019).

82. Goddard, T. D. *et al.* UCSF ChimeraX: Meeting modern challenges in visualization and analysis. *Protein Sci.* **27**, 14–25 (2018).

83. Pettersen, E. F. *et al.* UCSF Chimera—A visualization system for exploratory research and analysis. *J. Comput. Chem.* **25**, 1605–1612 (2004).

84. Margineanu, A. *et al.* Complexation of Lipofectamine and Cholesterol-Modified DNA Sequences Studied by Single-Molecule Fluorescence Techniques. (2007) doi:10.1021/bm700486q.

FIGURE LEGENDS:

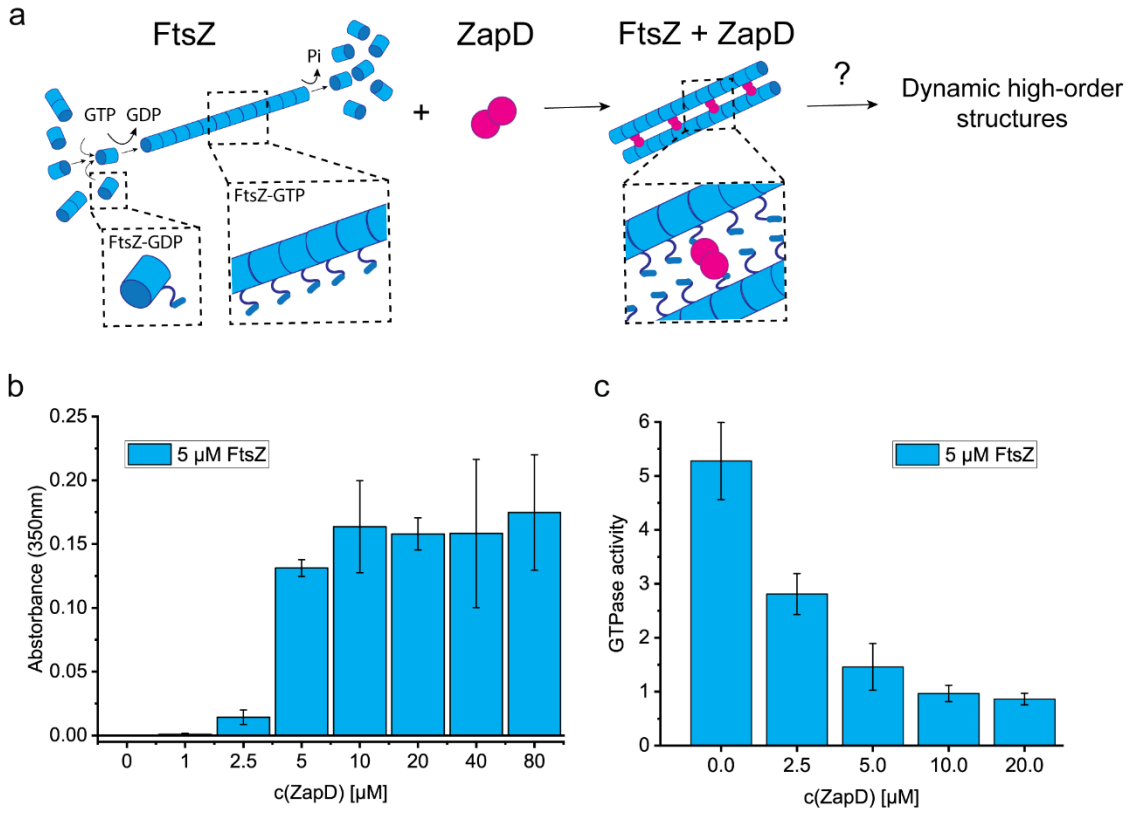

Figure 1. ZapD binds FtsZ and promotes filament bundling. **a** Scheme of the FtsZ protein and its interaction with ZapD. E. coli FtsZ (blue) monomers in solution oligomerize depending on the buffer conditions. Upon GTP binding, FtsZ homopolymerizes directionally, assembling single stranded filaments. ZapD is a robust dimer (magenta) that interacts directly with FtsZ, crosslinking filaments by promoting lateral interactions between them. Although the molecular mechanism is still unclear, the current hypothesis of interaction assumes dimers of ZapD crosslinking two FtsZ filaments through the C-terminal region of FtsZ, expecting at around 2:1 (FtsZ:ZapD) molar ratio in an homogeneous bundle. According to this model, the orientation of the FtsZ filaments could be parallel or antiparallel, allowing the growth and treadmilling of the filaments. However, the mechanism of assembly of dynamic high-order structures is still unknown. **b** Turbidity assays measuring the absorbance at 350 nm of samples containing 5 µM FtsZ and increasing concentrations of ZapD. The turbidity of the sample was measured 5 minutes after the addition of 1 mM GTP at working buffer (50 mM KCl, 50 mM Tris-Cl, 5 mM $MgCl_2$ pH 7). FtsZ polymers do not show a significant turbidity at this wavelength; therefore, the signal at 350 nm corresponds to the presence of large FtsZ macrostructures and bundles. The mean value and SD of >3 independent replicates are plotted in the graph. **c** GTPase activity of FtsZ after addition of 1 mM GTP in presence of increasing concentrations of ZapD at working conditions (50 mM KCl, 50 mM Tris-Cl, 5 mM $MgCl_2$ pH 7). The mean value and SD plotted in the graph are the result of 3 independent replicates. The GTPase activity was measured as a result of the Pi released from GTP consumption. The units are Mol GTP consumed per Mol FtsZ per min.

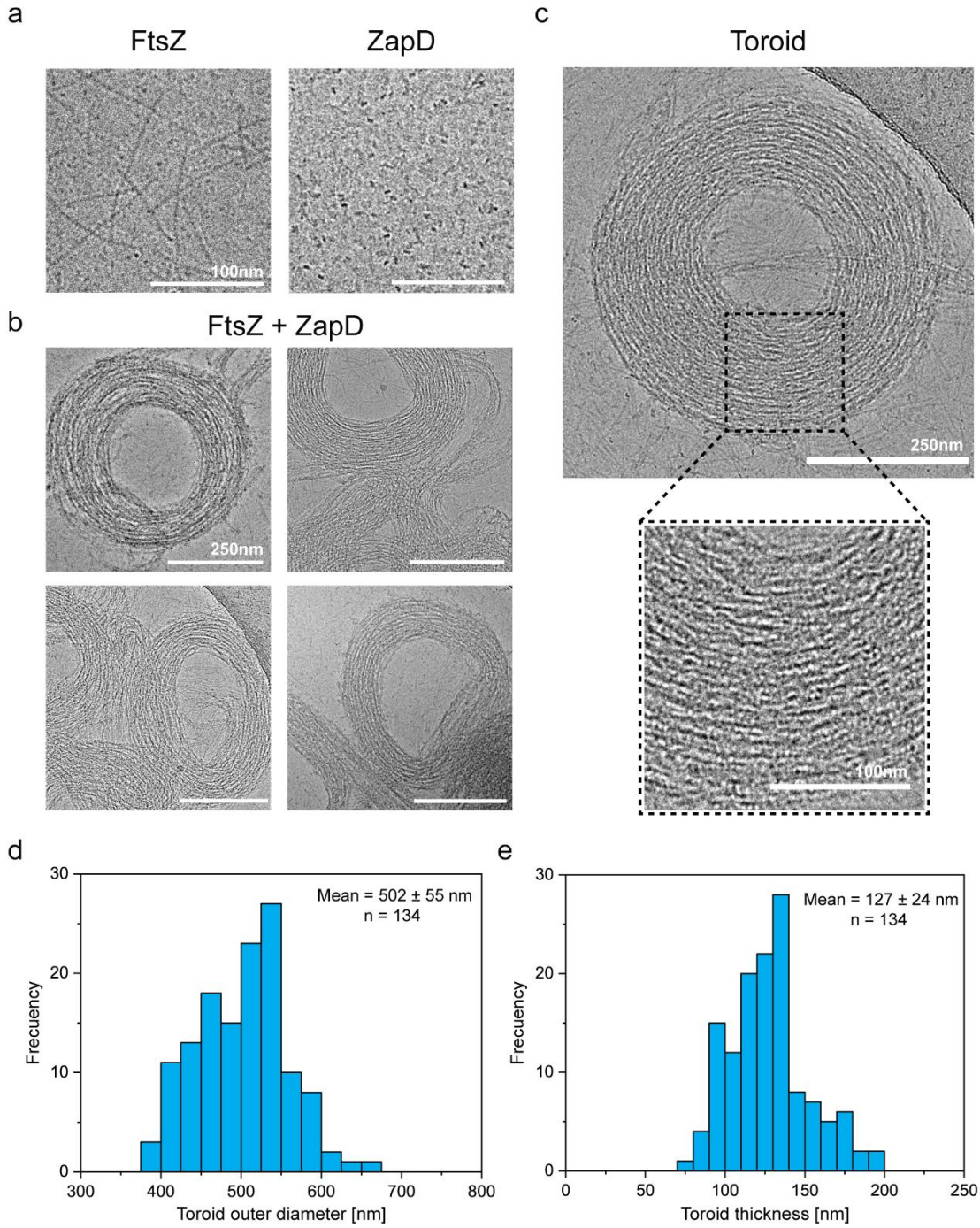

Figure 2. ZapD promotes the formation of FtsZ toroids. **a** Cryo-EM micrographs of FtsZ filaments (FtsZ-GTP form) (left) and ZapD protein (right) at 10 µM under working conditions (50 mM KCl, 50 mM Tris-Cl, 5 mM $MgCl_2$ pH 7). Scale bars are 100 nm **b** Cryo-EM images of FtsZ (10 µM) in the presence of equimolar concentrations of ZapD (ratio 1:1) and 1 mM GTP in working conditions. Cryo-EM grids were plunge frozen 2 min after GTP addition to favor the assembly of FtsZ and ZapD structures. The proteins were mixed before the polymerization was triggered by GTP addition. Scale bars are 250 nm. **c** Micrograph of an individual FtsZ toroid found under the same conditions as in (**b**). Close-up view of an area within the toroid is framed by a dotted black line, revealing the large amount of FtsZ filaments that form its structure. **d** Distribution of the outer diameter of the FtsZ toroid. Each toroid was measured perpendicularly in the shortest and longest axis to ensure the reliability of the measurement. The mean value and standard deviation are shown in the graph. **e** Distribution of toroidal thickness. It was measured as the result of the difference between the outer and inner diameter of each toroid. The mean value and standard deviation are shown in the graph.

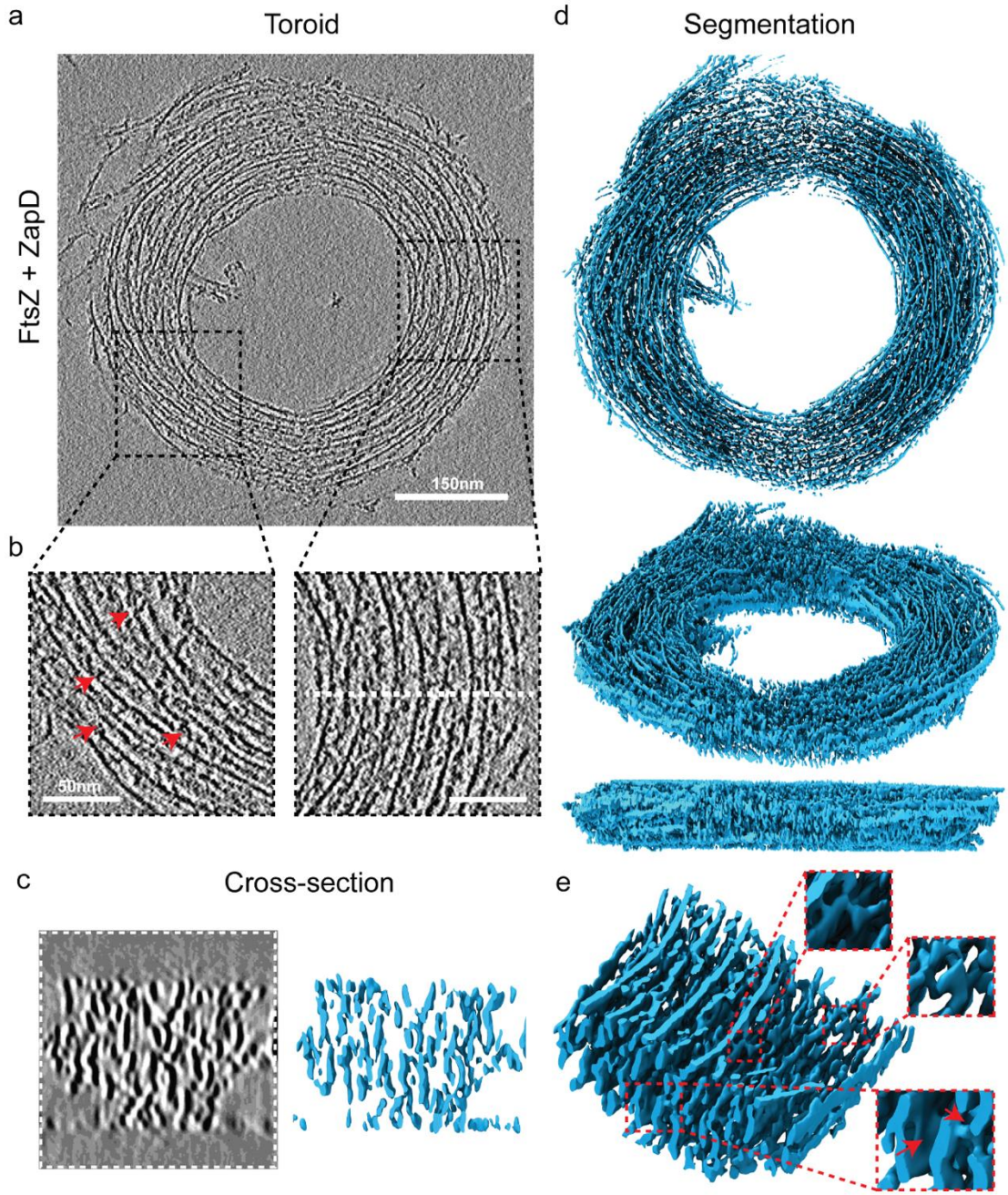

Figure 3. 3D structure of FtsZ toroids revealed by cryo-ET. a Representative micrograph of a FtsZ toroid resulting from the interaction of FtsZ with ZapD. The image is the average of five 6.4 nm thick tomographic slices (total thickness of 32 nm) of the reconstructed tomogram around the equatorial plane of a single FtsZ toroid. Scale bar is 150 nm. The concentrations of FtsZ and ZapD were 10 µM and 1 mM of GTP was added to trigger polymerization under working conditions (50 mM KCl, 50 mM Tris-Cl, 5 mM $MgCl_2$ pH 7). **b** Close-up views of the toroidal structure show the alignment of FtsZ filaments forming the toroid. Red arrows indicate the presence of connections between filaments. **c** Cryo-ET image (left) shows the cross-section corresponding to the area located at the white dotted line in **(b).** This image is the average of nine tomographic slices from the denoised tomogram. The isosurface of the cross-section (right) shows the alignment and organization of the FtsZ filaments within the toroid. This suggests a regular distribution of filaments assembling the toroid. FtsZ filaments are represented in blue. **d** Isosurface of the FtsZ toroid shown in (**a**). It was extracted from the reconstruction of the denoised tomographic volume and positioned in different views to facilitate its visualization: (top) front view, (middle) side view and (bottom) lateral view. **e** A

close-up view of the segmented toroidal structure. It shows the complex internal organization of filaments assembling the toroid. It corresponds to a zone within the toroid shown in **(d)**. Close-up views of the isosurface show different connections between filaments.

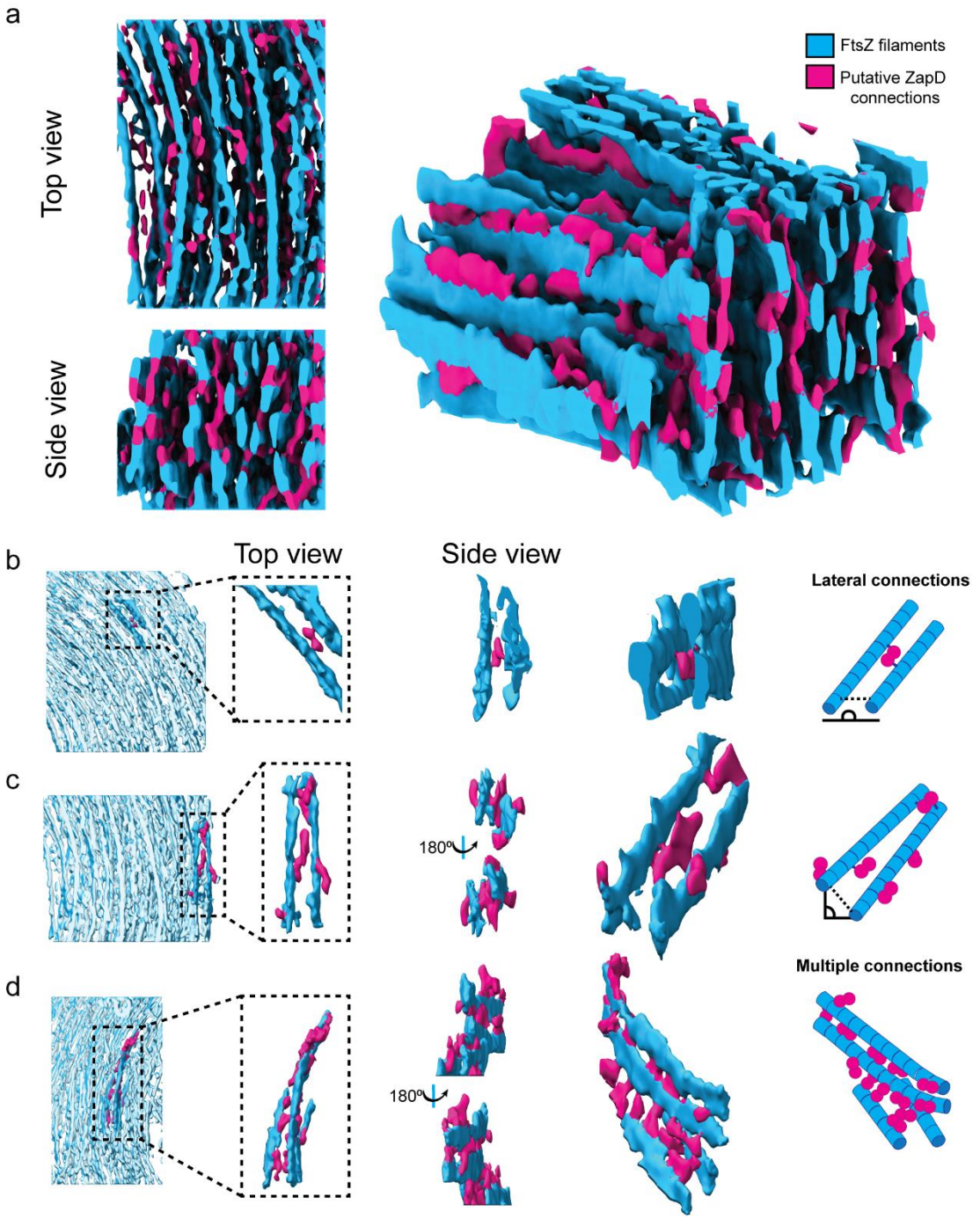

Figure 4. FtsZ filaments are connected by putative ZapD crosslinkers to assemble the toroidal structure. a Top (left, top), side (left, bottom) and lateral (right) views of the isosurface from an area within the toroidal structure shown in (Fig. 3a). The FtsZ filaments are colored blue, while filament connections or putative ZapD proteins are labelled magenta to facilitate interpretation of the results. Other putative ZapD proteins decorating the FtsZ filaments were not labelled in magenta because they were not forming any clear linkage between the filaments. **b-d** Different examples of connections between filaments by putative ZapD proteins within the toroid. Filaments are labelled in blue and putative ZapD in magenta to facilitate their interpretation. From left to right, the localization of the analyzed area, a close-up view of the structure of interest, different views of the crosslinkers and a schematic to illustrate the interpretation of the data. The schematic (right) represents the localization of ZapD proteins (magenta) and FtsZ filaments (blue). **b** Lateral connection of two FtsZ filaments by a putative

ZapD dimer. In this example, the attachment of each globular density or putative ZapD monomer was bound to each filament, allowing for a lateral bond. **c** Putative ZapD connections stabilizing two filaments by a lateral interaction. Additional ZapD decorations attached only to one of the filaments appear to be available for other filament linkages. **d** Multiple ZapD proteins can connect to filaments and stabilize the interaction. First, the two upper filaments are connected to each other by lateral connections through several putative ZapD. The lower filament connects laterally with the two other filaments. In the upper part, additional decorations or putative ZapD proteins would be available to establish further interactions forming a three-dimensional mesh.

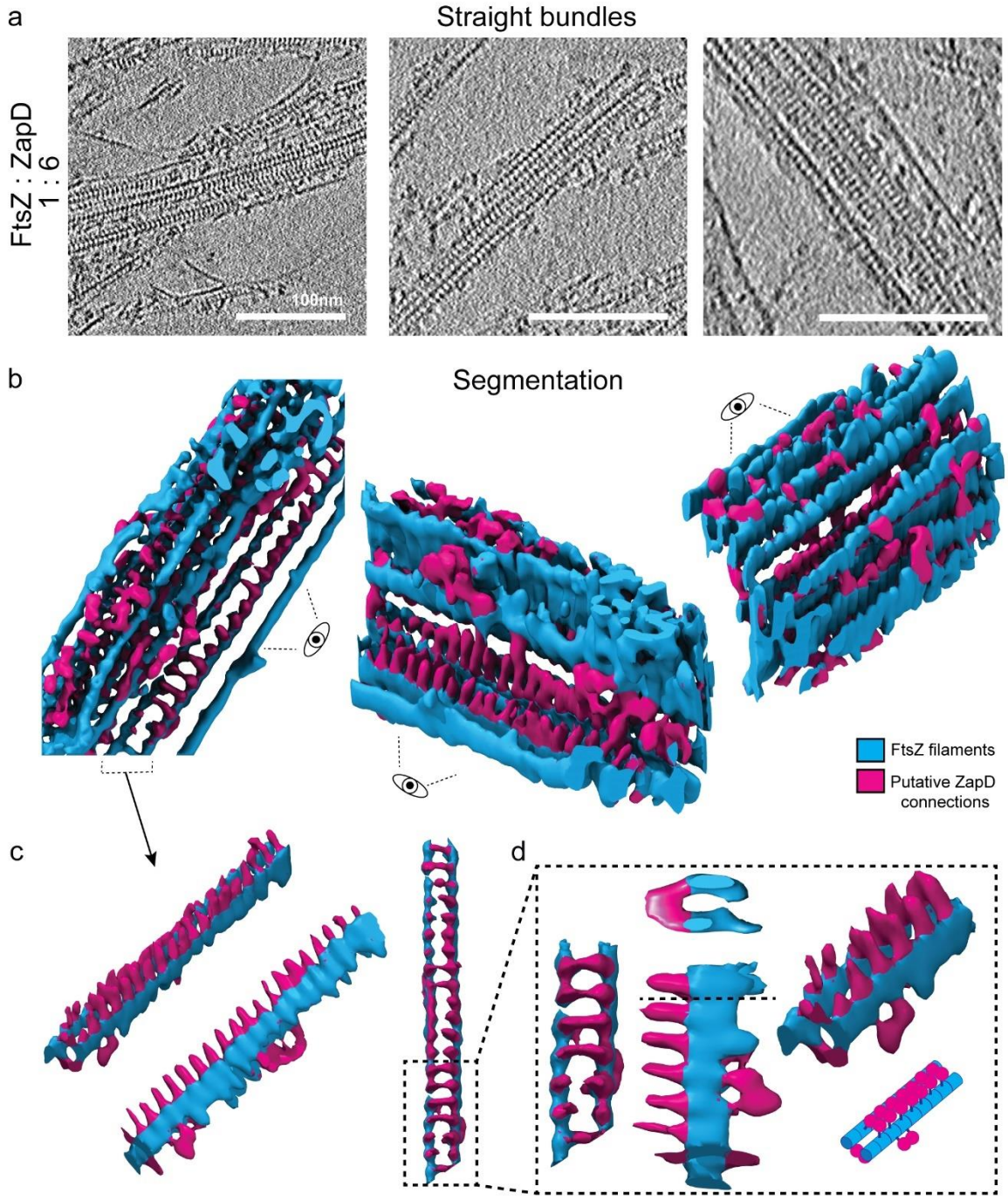

Figure 5. Formation of straight FtsZ bundles is driven by high ZapD binding. a Representative images of straight FtsZ bundles resulting from the interaction of FtsZ with high ZapD concentrations under working conditions (50 mM KCl, 50 mM Tris-Cl, 5 mM $MgCl_2$ pH 7). The concentrations of FtsZ and ZapD were 10 µM and 60 µM, respectively, and 1 mM of GTP was added to trigger polymerization. The straight bundles were only found at high ZapD concentrations. The image is the average of five 6.4 nm thick tomographic slices (total thickness of 32 nm) of the reconstructed tomogram. Scale bars are 100 nm. **b** Isosurface of the straight bundles from the denoised tomographic volume. FtsZ filaments are colored in blue and putative ZapD connections in magenta. Three different views (top (left) and side views (middle, right)) are shown. Straight bundles are organized in a regular organization. Multiple bonds between filaments are found in a very regular manner; putative ZapD proteins align and stack to stabilize two FtsZ filaments by crosslinking them. In addition, lateral connections were

also found linking couple of stabilized filaments among them, ultimately assembling the straight bundle. **c** Different views of one of the isolated filaments from the straight bundle. A side view of the filaments (middle) shows a spike-like structure regularly located at the top of the FtsZ filaments, connecting them as observed in the top view (right). **d** Different close-up views of the filament structure shown in **(c).** In the cross-section of the structure (middle, top), it is clearly visible that the ZapD proteins connect the two filaments, forming a bridge over them. A schematic of the suggested interaction (right, bottom) shows the location of putative ZapD dimer in this structure.

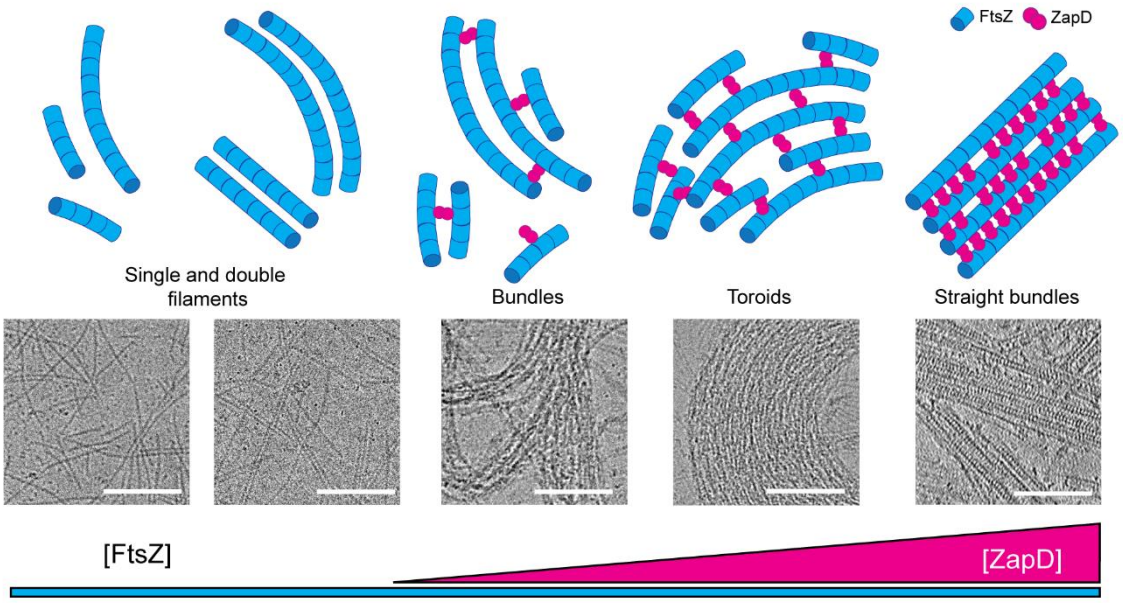

Figure 6. Density of ZapD connections modulate the spatial organization of FtsZ filaments into high-order structures. (Top) Scheme of the FtsZ FtsZ high-order structures formed in the presence of increasing ZapD concentrations. (Bottom) Cryo-EM images of the structures represented in the schemes. FtsZ filaments can interact laterally with each other, forming single and double filaments upon GTP binding. At low concentrations of ZapD, only a few lateral connections are formed and thus no bundles can be assembled. However, at higher ZapD concentrations, more ZapD-mediated bonds are established, favouring the formation of bundles. Higher ZapD binding densty promotes the assembly of toroidal structures. A further increment in the number of ZapD connections, the bundle is enriched on ZapD binding density, which straightens up the filaments allowing the formation of straight bundles. The assembly of FtsZ high-order structures is dependent on the number of lateral crosslinking through ZapD dimers and some intermediate states are expected between the structures shown. Scale bars are 100 nm.